ENHANCEMENT OF NEAR-FRONT APPROXIMATION FOR LINEAR FRACTURE ANALYSIS BY BIEM

Tarit Rung-aree[1], and Jaroon Rungamornrat[1,*]

[1] Applied Mechanics and Structures Research Unit, Department of Civil Engineering, Faculty of Engineering, Chulalongkorn University, Bangkok, Thailand 10330.

*Corresponding author address: Jaroon.r@chula.ac.th

Abstract

This paper presents a simple procedure to enhance the near-front approximation in the stress analysis of a three-dimensional, isotropic, linearly elastic, cracked medium by the boundary integral equation method. The information of the asymptotic crack-front behavior is utilized as the basis for the enhancement of the approximation of the relative crack-face displacement. Two different schemes are proposed in the present study. In the first scheme, the available 9-node crack-tip elements are generalized by adopting the p-refinement in the direction perpendicular to the crack front. This clearly enables the resulting crack-tip elements to accurately capture high-order terms in the asymptotic near-front expansion of the relative crack-face displacement without the need to reduce the size of the elements. The invented crack-tip elements with the p-refinement can then be utilized along with the standard elements with the h-refinement without the deterioration of the accuracy. The second scheme is based upon the use of available 9-node crack-tip elements together with the newly invented elements, termed back crack-tip elements, in the approximation of the relative crack-face displacement. The idea is to supply the square-root feature from the asymptotic crack-front field to the crack-tip elements and the elements behind them. In this way, the size of a region on the crack surface where the square-root behavior is captured accurately will not be reduced when the uniform h-refinement is employed to improve the solution accuracy. The two proposed elements are successfully implemented within the framework of a weakly singular symmetric Galerkin boundary element method. A selected set of results is then reported to demonstrate the computational performance of the proposed elements.

Keywords: Boundary Integral Equation Methods, Back Crack-tip Elements, Crack-tip Elements, Relative Crack-face Displacement, Stress Intensity Factors

1. INTRODUCTION

Fracture-induced failure is a typical mode of failures commonly found in various engineering components and structures, especially for those made of brittle materials or materials with relatively low fracture toughness. The design of those structures to ensure their integrity and safety clearly requires ones to take such failure mode into consideration. To provide the sufficient basis in assisting the design procedure, the fundamental understanding of the fracture failure is required a priori, and it can be achieved through various approaches including theoretical simulations based upon a well-known theory of fracture mechanics.

The modeling of pre-existing flaws and damages in materials in a form of cracks via the theory of linear elastic fracture mechanics (LEFM) is standard and has been adopted extensively in the study of brittle fractures.

Within the framework of LEFM, the determination of stress intensity factors (SIFs) is a crucial task in the stress analysis of cracked bodies. Those fracture parameters, which provide the complete description of the dominant elastic field in the vicinity of the crack front, are essential and serve as fundamental data in various models to simulate fracture-related responses including the crack growth initiation and directions of propagation. Although the numerical techniques based upon the standard finite element method (FEM) and boundary integral equation method (BIEM) have been found capable of and extensively employed in performing the linear fracture analysis, the singularity nature of the stress field along the crack front [1] still poses challenging issues associated with the accuracy and efficiency of near-front approximation and the post-process for the SIFs. It has been well recognized that standard elements with polynomial-

based shape functions has limited capability in discretizing the near-front field induced by the embedded singularity, and it generally requires extremely fine meshes to achieve the specified accuracy. To handle such difficulty, the direct integration of the right structure of the near-front field in the development of local interpolation functions is considered an attractive alternative.

Within the framework of boundary integral equation method (BIEM), various types of crack-tip elements have been implemented and used in the linear fracture analysis. Luchi and Rizzuri [2] proposed an 8-node traction singular boundary element to account for the stress singularity in the stress analysis of three-dimensional crack bodies by the displacement integral equation and the subdomain technique. Mi and Aliabadi [3] introduced special crack-tip elements with the discontinuous shape functions to approximate the crack-face displacement adjacent to the crack front in the hypersingular dual boundary element method for three-dimensional crack problems. Later, Li et al. [4] developed a special crack-tip element by directly integrating the right asymptotic structure of the near-front relative crack-face displacement in the element shape function. Such elements were then implemented in the framework of the weakly singular symmetric Galerkin boundary element method (SGBEM) for the analysis of cracks in three-dimensional, linear elastic media. While adopting those special elements along the crack-front can significantly enhance the accuracy of the approximation by using reasonably coarse meshes, the work was still limited to bodies made of isotropic materials. A 3-node singular crack-tip element that can exactly represents the strain singularity was later adopted by Kebir et al. [5] in the collocation-based dual boundary element method for the simulation of mixed-mode crack growth of bolted joints. A family of 9-node crack-tip elements was also developed by Pan and Yuan [6] in the development of the single-domain boundary element method for the analysis of three-dimensional, anisotropic, cracked media. The hypersingular integral equations were employed in their formulation together with the collocation-based solution scheme. Later, Grey et al. [7] integrated the constraint on

the relative crack-face displacement to obtain an improved version of quarter-point elements, and then used them in the two-dimensional, linear fracture analysis by a hypersingular SGBEM. Rungamornrat and Mear [8] also extended the work of Li et al. [4] for both the integral formulation and the near-front approximation to handle the material anisotropy. Xie et al. [9] generalized the work of Mi and Aliabadi [3] to establish a 9-node crack-tip element with one or two of their edges being aligned with the crack front. The performance of the proposed element was investigated within the framework of a hypersingular, collocation-based, dual boundary element method. Most recently, Xie et al. [10] proposed a novel triangular crack-tip element for the fracture analysis by BIEM that can properly capture the square-root asymptotic behavior. In the development of such element, a distance function to the crack edge was employed together with the element shape functions of 8-node serendipity elements.

While various types of crack-tip elements were developed and successfully implemented within the framework of BIEMs, evidences from the past studies have indicated that the need for further development regarding the approximation of the near-front field is still required. For instance, the use of special crack-tip elements together with the uniform mesh refinement scheme can lead to the undesirable convergence behavior (e.g., [11-12]); in particular, finer meshes can yield less accurate results than coarser ones. The same behavior was also pointed out by Rungamornrat et al. [13] when the solved relative crack-face displacement data was further used in the determination of the T-stress. This is due to the fact that as the mesh is uniformly refined, the region adjacent to the crack front, where the asymptotic behavior is accurately captured by the crack-tip elements, becomes smaller. Although the remaining larger region of the crack surface is also refined, the quality of the approximation of standard elements is not as good as the crack-tip elements especially for the region relatively close to the crack front. To avoid this problem, Rungamornrat et al. [13] suggested that finer meshes are required in the region on the back of the crack-tip elements to supply the

การประชุมวิชาการวิศวกรรมโยธาแห่งชาติ ครั้งที่ 26
วันที่ 23-25 มิถุนายน 2564, การประชุมรูปแบบออนไลน์

NCCE26
BEYOND THE LIMIT

The 26th National Convention on Civil Engineering
23-25 June 2021, Online Conference

comparable level of accuracy.

In the present study, a simple approach is proposed to handle the problem described above. Two novel types of elements, the crack-tip element and the back crack-tip element, are constructed based upon the right structure of the near-front relative crack-face displacement and then implemented within the framework of three-dimensional, weakly singular SGBEM. The performance of the developed elements in the context of both *p*- and *h*-refinement schemes is demonstrated.

2. PROBLEM FORMULATION

Consider a three-dimensional infinite body Ω containing isolated cracks as shown in Fig. 1. The medium is made of a homogeneous, isotropic, linearly elastic material and free of the body force and remote loading. The crack surface is described by two geometrically coincident surfaces S^+ and S^- with the outward unit normal vectors $\boldsymbol{n}^+$ and $\boldsymbol{n}^-$, respectively. The cracked medium is loaded by a self-equilibrated crack-face traction $\boldsymbol{t}^{0+} = -\boldsymbol{t}^{0-}$.
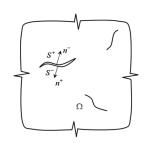

Figure 1   Schematic of elastic whole space containing isolated cracks.

The boundary value problem of the cracked medium shown in Fig.1 can be formulated in a form of boundary integral equations by choosing the relative crack-face displacement $\Delta u_j = u_j^+ - u_j^-$ as the primary unknown. By following the work of Rungamornrat and Mear [8], the relative crack-face displacement Δu_j is governed by a weakly singular, weak-form traction integral equation:

$$-\frac{1}{2}\int_{S^+}\tilde{u}_k(\boldsymbol{y})\Delta t_k^0 dA(\boldsymbol{y}) = \quad (1)$$
$$\int_{S^+}D_t\tilde{u}_k(\boldsymbol{y})\int_{S^+}C_{mj}^{tk}(\boldsymbol{\xi}-\boldsymbol{y})D_m\Delta u_j(\boldsymbol{\xi})dA(\boldsymbol{\xi})\,dA(\boldsymbol{y})$$

where standard indicial notation applies throughout, in particular, lower case indices range from 1 to 3 and repeated indices imply the summation over their range; $\tilde{u}_k$ is a sufficiently smooth test function; $\Delta t_k^0 = t_k^{0+} -$

t_k^{0-} is jump in the crack-face traction; $D_m(\cdot) = \varepsilon_{mps}n_p\partial(\cdot)/\partial\xi_s$ is a surface differential operator; and $C_{mj}^{tk}(\boldsymbol{\xi}-\boldsymbol{y})$ is a singular kernel defined explicitly by

$$C_{mj}^{tk}(\boldsymbol{\xi}-\boldsymbol{y}) = \frac{\mu}{4\pi(1-\nu)r}\cdot\Big[(1-\nu)\delta_{tk}\delta_{mj} + \quad (2)$$
$$2\nu\delta_{km}\delta_{tj} - \frac{(\xi_k-y_k)(\xi_j-y_j)}{r^2}\delta_{tm}\Big]$$

where $r = \|\boldsymbol{\xi}-\boldsymbol{y}\|$; ν is Poisson's ratio; μ is the elastic shear modulus; and δ_{tj} denotes a standard Kronecker-delta symbol. The kernel function $C_{mj}^{tk}(\boldsymbol{\xi}-\boldsymbol{y})$ is singular only at $\boldsymbol{\xi} = \boldsymbol{y}$ of order $1/r$ as $r \to 0$ and, as a result, all involved integrals in Eq. (1) are integrable in the sense of Riemann sum.

3. SOLUTION SCHEME

A well-known, weakly singular SGBEM is implemented to construct numerical solutions of Eq. (1). Standard Galerkin approximation together with the finite element procedure is utilized to discretize the trial function Δu_j and the test functions $\tilde{u}_k$ into

$$\Delta u_j(\boldsymbol{y}) = \sum_{p=1}^N u_j^{\Delta(p)}\boldsymbol{\phi}^{(p)}(\boldsymbol{\xi}); \quad (3)$$
$$\tilde{u}_k(\boldsymbol{y}) = \sum_{p=1}^N \hat{u}_k^{(p)}\boldsymbol{\phi}^{(p)}(\boldsymbol{y})$$

where $\boldsymbol{\phi}^{(p)}$ is the nodal basis function associated with the pth node; $u_j^{\Delta(p)}$ are nodal degrees of freedom at the pth node; $\hat{u}_k^{(p)}$ are arbitrary constants at the pth node; and N denotes the number of nodes resulting from the discretization. Due to the weakly singular nature of the boundary integral equation (1), the nodal basis functions $\boldsymbol{\phi}^{(p)}$ is only required to be continuous and they can be constructed in an elementwise fashion following standard finite element procedure. In the present study, standard C^0 isoparametric elements are employed to discretize the majority of the crack surface except the region close to the crack front where proposed crack-tip elements are adopted. Substituting Eq. (3) into Eq. (1) yields the following system of linear algebraic equations:

$$\mathbf{C}\Delta\mathbf{U} = \mathbf{T}^0 \quad (4)$$

where entries of the coefficient matrix $\mathbf{C}$, the vector of nodal degrees of freedom $\Delta\mathbf{U}$, and the prescribed vector $\mathbf{T}^0$ are defined explicitly by

$$[\mathbf{C}]_{3(p-1)+i,3(q-1)+j} = \quad (5)$$
$$\int_{S^+}D_t\phi^{(p)}(\boldsymbol{y})\int_{S^+}C_{mj}^{ti}(\boldsymbol{\xi}-\boldsymbol{y})D_m\phi^{(q)}(\boldsymbol{\xi})dA(\boldsymbol{\xi})\,dA(\boldsymbol{y})$$

การประชุมวิชาการวิศวกรรมโยธาแห่งชาติ ครั้งที่ 26
วันที่ 23-25 มิถุนายน 2564, การประชุมรูปแบบออนไลน์

NCCE26
BEYOND THE LIMIT

The 26th National Convention on Civil Engineering
23-25 June 2021, Online Conference

$$[\Delta \mathbf{U}]_{3(q-1)+j} = u_j^{\Delta(q)} \tag{6}$$

$$[\mathbf{T}^0]_{3(p-1)+i} = -\frac{1}{2}\int_{S^+} \phi^{(p)}(\mathbf{y})\Delta t_i^0(\mathbf{y})dA(\mathbf{y}) \tag{7}$$

The coefficient matrix $\mathbf{C}$ and the known vector $\mathbf{T}^0$ are constructed in an efficient manner through a standard assembly procedure. The numerical evaluation of all involved weakly singular and nearly single double surface integrals over a pair of elements is achieved by adopting a special quadrature based on the integrand regularization via variable transformations and Gaussian quadrature rule [14]. The final system of linear equations (4) is then solved by a selected indirect linear solver such as a conjugate gradient method.

4. ENHANCEMENT OF NEAR-FRONT APPROXIMATION

It is well known that the relative crack-face displacement in the vicinity of the crack front exhibits a square-root type behavior, and this must be treated appropriately in the approximation. From the work of Rungamornrat et al. [13], the relative crack-face displacement possesses the following structure

$$\Delta \mathbf{u} = \sqrt{r}(\boldsymbol{\alpha}_0 + \boldsymbol{\alpha}_1 r + \boldsymbol{\alpha}_2 r^2 + \dots) \tag{8}$$

in which r denotes the distance in the direction perpendicular to the crack front and $\boldsymbol{\alpha}_i$ are constant vectors. It is apparent from (8) that the solution of $\Delta \boldsymbol{u}$ can be represented by a product of a square-root function $\sqrt{r}$ and a regular function of r. The structure of $\Delta \boldsymbol{u}$ was directly integrated to construct the 9-node crack-tip elements in the work of [4, 8]. Nevertheless, such elements can capture only the first three terms of the asymptotic expansion in Eq. (8).

In the present study, the 9-node crack-tip element developed by [4, 8] is extended via the *p*-refinement scheme (i.e., a scheme to enhance the approximation via the increase in the degree of polynomials in the element shape functions) to allow more terms in the expansion in Eq. (8) to be captured. In particular, the degree of polynomials used in the approximation is augmented by increasing the number of nodes in the direction normal to the crack front as shown in Fig. 2 while still maintaining the square-root feature. The final element shape function of the crack-tip element is given explicitly by

$$\bar{\psi}_{(i)}(\xi,\eta) = \frac{\sqrt{1+\eta}}{A_i}\psi_{(i)}(\xi,\eta) \tag{9}$$

$$A_i = \begin{cases} 1/2 & \eta_{(i)} = -1 \\ \sqrt{1+\eta_{(i)}} & \eta_{(i)} \neq -1 \end{cases} \tag{10}$$

where $\psi_{(i)}$ are standard shape functions of a Lagrange element containing $3\times(2+n_m)$ nodes resulting from the product between one-dimensional Lagrange polynomials corresponding to the number of nodes in each direction; $n_m > 0$ denotes the number of interior nodes in the direction perpendicular to the crack front; and the side $\eta = -1$ correspond to the crack front. In this sense, the extended element shape functions can capture the first $2+n_m$ terms in the expansion in Eq. (8).
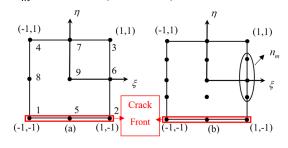

Figure 2 Schematic of master crack-tip element containing (a) 9 nodes and (b) $3\times(2+n_m)$ nodes. The side indicated by $\eta = -1$ denotes the crack front.

Another type of elements, termed here a "back crack-tip element", is implemented along with the available 9-node crack-tip elements to enhance the approximation of the near-front relative crack-face displacement. The idea is to supply the square-root feature from the asymptotic structure of the near-front field in Eq. (8) to not only the crack-tip elements located along the crack-front but also the elements behind them (i.e., the back crack-tip elements). In this way, the crack front region where the square-root behavior is properly captured will not be reduced when the uniform *h*-refinement (i.e., a scheme to enhance the approximation via refining the element size or increasing the number of elements in the finite element mesh) is adopted. The final shape functions for the 9-node back crack-tip element, with the master element shown in Fig. 2(a) and the side $\eta = -1$ representing the side closest to the crack-front, are taken as

$$\bar{\psi}_{(i)}(\xi,\eta) = \frac{\sqrt{2n_b+1+\eta}}{\sqrt{2n_b+1+n_{(i)}}}\psi_{(i)}(\xi,\eta) \tag{11}$$

where n_b denotes the order of the row of the back crack-tip elements counted from the first row adjacent to the crack-tip element.

In the analysis, two following refinement schemes for crack-tip elements are proposed. In the first scheme (*p*-refinement), the size of the crack-tip elements in the direction perpendicular to the crack front is maintained whereas the number of interior nodes n_m in the same direction is increased as shown schematically in Fig. 3(a). For the second scheme (*h*-refinement), the 9-node crack-tip elements are used and refined into smaller 9-node crack-tip elements and one or several layers of 9-node back crack-tip elements as illustrated in Fig. 3(b).
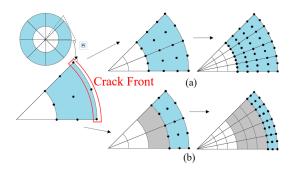

Figure 3   Schematic of two refinement schemes: (a) *p*-refinement of crack-tip elements (highlighted in blue) and (b) *h*-refinement of 9-node crack-tip elements into 9-node crack-tip (highlighted in blue) and back crack-tip elements (highlighted in grey).

5.   POSTPROCESS FOR STRESS INTENSITY FACTORS

Once the relative crack-face displacement is solved, such data is directly used together with the explicit extrapolation-free formula proposed by Rungamornrat and Mear [8] to compute the stress intensity factors (SIFs). The integration of the right asymptotic behavior into the crack-tip elements allows the post-process for the SIFs in terms of the extra degrees of freedom located along the crack front.

6.   NUMERICAL RESULTS

The computed SIFs and relative crack-face displacement of a penny-shaped crack embedded in an isotropic, elastic whole space under uniformly distributed normal and shear tractions are first compared with available exact solutions [15] to verify the proposed elements within the framework of weakly singular SGBEM. The enhancement of the near-front approximation via the two refinement schemes is then investigated by comparing computed stress intensity factors with those generated from the uniform *h*-refinement scheme without the back crack-tip elements. In particular, the rate of convergences with respect to the L²-norm of the error of the relative crack-face displacement for all three refinement schemes are also obtained and compared.

Consider a penny shaped crack of radius a contained in an isotropic elastic whole space with its surface oriented perpendicular to x_3-axis as shown in Fig. 4. The medium is loaded on the crack surface by either a uniformly distributed normal traction σ_0 or shear traction τ_0 in the x_1 direction as illustrated in Fig. 5.
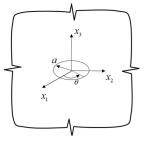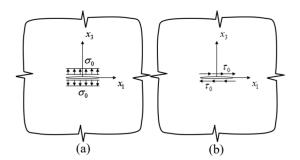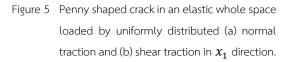

Figure 4   Schematic of a penny shape crack of radius a embed in unbounded domain.

Figure 5   Penny shaped crack in an elastic whole space loaded by uniformly distributed (a) normal traction and (b) shear traction in x_1 direction.

In the analysis, the crack surface is first divided into two regions. The region adjacent to the crack front is discretized by the proposed elements via the three refinement schemes whereas the remaining region is discretized by standard 6-node and 9-node isoparametric

การประชุมวิชาการวิศวกรรมโยธาแห่งชาติ ครั้งที่ 26
วันที่ 23-25 มิถุนายน 2564, การประชุมรูปแบบออนไลน์

NCCE26
BEYOND THE LIMIT

The 26th National Convention on Civil Engineering
23-25 June 2021, Online Conference

C^0-elements. Three meshes based upon the *p*-refinement of the crack-tip elements (Scheme-1), the *h*-refinement of the 9-node crack-tip and 9-node back crack-tip elements (Scheme-2), and the *h*-refinement of the 9-node crack-tip and standard elements (without the back crack-tip elements, Scheme-3) are shown in Fig. 6(a), (b) and (c), respectively. The first mesh of each scheme are chosen to be identical with the region adjacent to the crack front being discretized by a single layer of 9-node crack-tip elements. The crack-tip elements (blue elements) in the Mesh-2p and Mesh-3p contain 12 and 15 nodes, respectively; the Mesh-2h and Mesh-3h contain one layer and three layers of back crack-tip elements (grey elements), respectively; and the Mesh-2 and Mesh-3 are similar to the Mesh-2h and Mesh-3h with the back crack-tip elements being replaced by the standard elements.
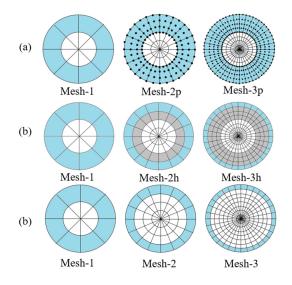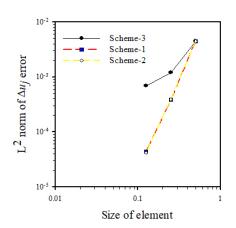

Figure 6 Three meshes of penny shaped crack adopted in the analysis: (a) scheme-1, (b) scheme-2, and (c) scheme-3 where crack-tip elements and back crack-tip elements are highlighted in blue and grey, respectively.

For the crack subjected to the uniformly distributed normal traction, only the mode-I SIF is non-zero and it is constant along the crack front. The percent errors of computed mode-I SIFs (relative to the exact solution reported in [15]) are reported in Table 1 for all three schemes (i.e., Scheme-1, Schem-2, and Scheme-3). It is evident that results obtained for all cases are in excellent with the benchmark solutions; in particular, the error is

less than 0.05% for all meshes. While the SIFs computed from the Scheme-1 are already accurate with the error less than a fraction of one percent, the improvement of the solution upon the refinement is not confirmed. Use of the Scheme-1 and Scheme-2 based upon the proposed elements yield the better convergence behavior; clearly, the percent error decreases as the mesh is refined. To further demonstrate the rate of convergence of the proposed schemes, the L^2-norms of the error of the relative crack-face displacement are plotted against the size of elements in Fig. 7 where the size of element in each mesh is the length of the side which perpendicular to the crack front of the element behind the crack-tip element. The computed rates of convergence of results obtained from the Scheme-1 and the Scheme-2 are approximately 3.126 and 3.229, respectively, and they are significantly improved from that for the Scheme-3 (approximately 0.929).

Figure 7 L^2-norm of error of the relative crack-face displacement versus the size of element in logarithmic scale for penny-shaped crack under uniformly distribution normal traction.

Table 1 The percent errors of computed mode-I SIFs of penny shaped crack subjected to uniformly distributed normal traction.

Mesh	Scheme-1	Scheme-2	Scheme-3
1	0.02400	0.02400	0.02400
2	0.01145	0.00967	0.02932
3	0.00613	0.00702	0.03818

For the crack under the uniform shear traction, only the mode-II and mode-III SIFs are non-zero and they vary along the crack front. The percent errors of computed non-zero mode-II and mode-III SIFs at θ = 0°, 45° and 90° (where θ is an angle measured from the x_1-axis and used to parameterize the crack front) are reported in Table 2 and 3, respectively. Again, the computed SIFs from the Scheme-1 and Scheme-2 agree very well with the exact solution [15] and more accurate than those obtained from the Scheme-3. The computed L^2-norm of the error of the relative crack-face displacement are also reported as a function of the size of elements in Fig 9 for all three schemes. Similar to the previous loading case, the estimated rates of convergence from the Scheme-1 and Scheme-2 are approximately the same (i.e., 3.087 and 3.197) and significantly higher than that of the Scheme-3 (i.e., 0.928). It should be pointed out that the significant improvement of both the accuracy of the computed SIFs and the rate of convergence of the numerical solutions results directly from the use of the two proposed elements in the approximation of the near-front field.

Table 2   The percent errors of computed mode-II SIFs of penny shaped crack subjected to uniformly distributed shear traction

θ	Mesh	Scheme-1	Scheme-2	Scheme-3
	1	0.14614	0.14614	0.14614
0	2	0.07081	0.08813	0.13484
	3	0.07006	0.08362	0.12354
	1	0.14488	0.14488	0.14488
45	2	0.07244	0.08842	0.13529
	3	0.06392	0.08416	0.12464

Table 3   The percent error of computed mode-III SIFs of penny shaped crack subjected to uniformly distributed shear traction

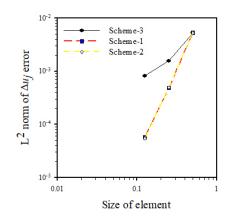| θ	Mesh	Scheme-1	Scheme-2	Scheme-3
	1	0.07762	0.07762	0.07762
45	2	0.00609	0.00152	0.04566
	3	0.00152	0.00000	0.04261
	1	0.08717	0.08717	0.08717
90	2	0.00108	0.00108	0.04197
	3	0.00108	0.00108	0.04627

Figure 8 L^2-norm of error of the relative crack-face displacement versus the size of element in logarithmic scale for penny-shaped crack under uniformly distribution shear traction

7.   CONCLUSIONS

A simple approach, via the use of crack-tip and back crack-tip elements, has been proposed to enhance the near-front approximation in the stress analysis of three-dimensional, isotropic, linearly elastic, cracked media by a weakly single SGBEM. The two special elements have been constructed by integrating the right structure of the near-front relative crack-face displacement. The existing 9-node crack-tip element has been modified to enable the adjustment of the number of nodes in the direction normal to the crack front. This therefore allows the crack-tip element to capture more terms in the asymptotic expansion. The 9-node back crack-tip element, after its shape function were enriched by the square-root function, can be used along with the 9-node crack-tip element in the h-refinement scheme without the reduction of the region on the crack surface where the square-root behavior is captured correctly.

Results from an extensive numerical study have confirmed that the use of either the crack-tip elements with the p-refinement scheme or the 9-node crack-tip and back crack-tip elements with the h-refinement scheme provides the significant improvement of the accuracy of the computed SIFs and the rate of convergence of the relative crack-face displacement compared with the case of a uniform h-refinement scheme with only 9-node crack-tip elements.

9. REFERENCES

[1] Williams M.L. (1957). On the stress distribution at the base of a stationary crack. *Journal of Applied Mechanics* **24**, 109–114.

[2] Luchi M.L., Rizzuri S. (1987) Boundary elements for 3D elastic crack analysis. *International Journal for Numerical Method in Engineering* **24**, 2553-2271. DOI: 10.1002/nme.1620241203

[3] Mi Y., Aliabadi M.H. (1994). Discontinuous crack-tip elements: application to 3d boundary element method. *International Journal of Fracture* **67**, 67–71. DOI: 10.1007/BF00016267

[4] Li S., Mear M. E., Xiao L. (1998). Symmetric weak-form integral equation method for 3D fracture analysis. *Computer Methods in Applied Mechanics and Engineering* **151**, 435-459. DOI: 10.1016/S0045-7825(97)00199-0

[5] Kebir H., Roelandt J.M., Foulquier J. (1999). A new singular boundary element for crack problems. *Engineering Fracture Mechanics* **62**(6), 497–510. DOI: 10.1016/S0013-7944(99)00008-9

[6] Pan E., Yuan F. G. (2000). Boundary element analysis of three-dimensional cracks in anisotropic solids. *International Journal for Numerical Methods in Engineering* **48**(2), 211–237. DOI: 10.1002/(SICI)1097-0207(20000520)48:2%3C211::AID-NME875%3E3.0.CO;2-A

[7] Gray L. J., Phan A.V., Paulino G.H., Kaplan T. (2003). Improved quarter-point crack tip element. *Engineering Fracture Mechanics* **70**, 269–283. DOI: 10.1016/S0013-7944(02)00027-9

[8] Rungamornrat J., Mear M. E. (2008). Weakly-singular, weak-form integral equations for cracks in three-dimensional anisotropic media. *International Journal of Solids and Structures* **45**(5), 1283-1301. DOI: 10.1016/j.ijsolstr.2007.09.030

[9] Xie G., Zhou F., Zhang D., Wen X., Li H. (2017). Calculation of stress intensity factor along the 3D crack front by dual BIE with new crack front elements. *Acta Mechanica* **228**, 1–19. DOI: 10.1007/s00707-017-1875-7

[10] Xie G., Zhou F., Zhang D., Wen X., Li H. (2019). A novel triangular boundary crack front element for 3D crack problems base on 8-node serendipity element. *Engineering Analysis in Boundary Element* **105**, 296-302. DOI: 10.1016/j.enganabound.2019.04.017

[11] Pham T. N. (2015). *Analysis of cracks in transversely isotopic, linear elastic half-space by weakly singular BIEM*. Master Thesis of Chulalongkorn University.

[12] Limwibul V. (2015). *Analysis of generalized T-stress for cracks in 3D linear piezoelectric media under various crack-face conditions by BEM*. Master Thesis of Chulalongkorn University.

[13] Rungamornrat J., Sukulthanasorn N., Mear M. E. (2019). Analysis for T-stress of cracks in 3D anisotropic elastic media by weakly singular integral equation method. *Computer Methods in Applied Mechanics and Engineering* **347**, 1004–1029. DOI: 10.1016/j.cma.2019.01.007

[14] Xiao L. (1998). *Symmetric weak-form integral equation method for three-dimensional fracture analysis*. Ph.D. Dissertation of Texas University.

[15] Fabrikant V.I. (1989). *Applications of potential theory in mechanics.* Kluwer Academic, Dordrecht, Netherland, 252-257.